IJMGE, Vol.50, No.2, (2016) 201–210

International Journal of Mining and Geo-Engineering

A laboratory study on mix design to properly resemble brittle jointed rock

M. Asadizadeh [a*], M. Farouq Hossaini [a], M. Moosavi [a], S. Mohammadi [a]

[a] *School of Mining Engineering, College of Engineering, University of Tehran, Tehran, Iran*

ARTICLE HISTORY

Received 27 Feb 2016, Received in revised form 25 May 2016, Accepted 03 Jul 2016

ABSTRACT

In this research attempts were made to create a mortar with relatively high uniaxial compressive strength (UCS), easy casting, high flexibility, instant hardening, low cost and easy availability. The main use of this material is to physically model the mechanical behavior of jointed rock-like blocks. The effect of four parameters such as joint roughness coefficient (JRC), bridge length (L), bridge angle (γ) and joint inclination (θ) on UCS of non-persistent jointed blocks were studied. For this purpose, 35 cylindrical specimens with a broad range of plaster content (P) and cement content (C) in different ages were tested. In order to increase the strength of blocky specimens, some amounts of retardant and lubricant agents were used. The results demonstrated that the utilization of 3 wt.% (weight percent) lubricant MGAR106 and 0.05 wt.% retardant decreases water content by 12.5% and increases plaster and cement content by 8.3% and 4.17% respectively. Consequently, UCS of blocky specimens increased by 284.33%. In order to formulate the effect of P/C content and also the age of cylindrical specimens (A) on compressive strength (UCS), Multivariate Non-linear Regression (MNR) and Bayesian Regularized Artificial Neural Network (BRANN) models were employed. The results showed that BRANN approach is able to provide more precise predictions of the specimen UCS compared to the results from MNR model. Moreover, P/C content had more impact on UCS than the specimen age had. Finally the UCS tests on blocky specimens indicated that an increasing in JRC, bridge length or bridge angle results in a rise in UCS; moreover UCS would be in its minimum when joint inclination was 60°. Furthermore, the capability of produced material to model cracking behavior of jointed blocks was verified.

Keywords: *Mixture plan. UCS test; Non-persistent joint; Regression modelling; Bayesian Regularization Neural Network*

1. Introduction

Physical modeling is one of the most robust methods to study cracking, mechanical and shear behavior of non-persistent jointed rock specimens. The effect of Joint Roughness Coefficient (JRC) on shear strength of non-persistent rock joints has not yet been investigated using physical modeling. The major difficulty in conducting these experiments, is to create mated non-persistent jointed specimens with specific JRC. Often two joint surfaces in natural rock are not the same as each other. But on the other hand, studying the effect of joint roughness, bridge length and bridge angle on the mechanical and shear behaviour of non-persistent joints requires discontinuities with same roughness. Therefore, in order to investigate the effect of rock joint roughness on mechanical and shear response of non-persistent jointed specimens, a specific mixture plan is required. Many researchers have used artificial specimen -so called 'rock-like' material- to investigate the influence of abovementioned parameters on specimens with open or close non-persistent smooth joints [1-14].

Gehle and Kutter's took advantages of pure gypsum to investigate breakage and shear behavior of intermittent rock joints [7]. Prudencio et.al utilized a mixture of fine sand, cement and distilled water, mixed in proportion of 4000/1000/1235 by weight to study the strength and failure modes of rock mass models with non-persistent joints [9]. Uniaxial and triaxial compression tests made with this mixture produced the following results: unconfined compressive strength σ_c=3.46 MPa after 14 days, cohesion 0.86 MPa, peak angle of friction 37°, tensile strength σ_t=0.45 MPa, tangent modulus of deformation E_{50}=2400 MPa, and Poisson's ratio 0.16. Ghazvinian et al. used a mixture of plaster (37.5%), cement (25%) and water (37.5%) to model the failure mechanism of planar non-persistent open joints [10]. Wong et.al used a mixture of barite, sand, plaster and water with a mass ratio of 2:4:1:1.5 to investigate crack coalescence in rock-like materials containing three flaws [11, 12]. The average values of specific weight, uniaxial compressive strength, tensile strength and friction coefficient of the modeling material were γ=17.67 KN/m3, σ_c=2.09 MPa, σ_t=0.35 MPa, and 0.62, respectively. Park and Bobet investigated crack coalescence in specimens with open and closed cracks using a mixture of Hydrocal B-11, a gypsum, diatomaceous earth and tap water [13]. The water and mass proportions used were water/gypsum = 0.4, and water/diatomaceous earth = 35.0. The uniaxial compression strength of non-jointed gypsum specimens was about 35 MPa. Huang et.al

* Corresponding author.
E-mail address: mostafa.asadizadeh@gamil.com (M. Asadizadeh).

DOI: 10.22059/ijmge.2016.59830
Journal Homepage: ijmge.ut.ac.ir

investigated fracture mechanical behavior of rock-like materials containing two unparalleled fissures under uniaxial compression utilizing rock-like specimens by compounding C42.5 cement, quartz sand, and water at a mass ratio of 1.0:0.8:0.35 [14].

Many researchers have applied Artificial Neural Networks (ANNs) and Multivariate Regression (MR) in the field of geotechnical engineering [15-19]. Recently Kumar et al. [15] predicted rock properties using MR and ANNs and by taking drill bit speed, penetration rate, drill bit diameter and sound level produced during drilling as input parameters. Esamaldeen et al. [16], used ANNs and the MR in order to predict UCS of banded amphibolite rocks. In this research micro-fabric properties including grain size, shape factor and quartz content were used as input parameters. An attempt was made to develop artificial neural network and multivariable regression analysis models in order to predict UCS of rock surrounding a roadway [17]. Rock mass deformation modulus was predicted utilizing ANN based on geotechnical log sheet data [18]. Rezaei et al. [19] developed two predictive models including soft computing methods and multivariable regression analysis to predict deformation modulus based on data obtained from dilatometer tests.

In this paper, synthetic rock-like material has been produced to investigate the strength behaviour of non-persistent jointed blocks, equivalent to soft rock. Mixtures with a wide range of Plaster content (P), Cement content (C) and specimen Age (A) were prepared and tested. The effect of additives and lubricants on blocky specimens was also studied. Furthermore, the influence of P, C content and A on UCS of cylindrical specimens was investigated; and two models including Multivariate Non-linear Regression (MNR) and Bayesian Regularization Artificial Neural Network (BRANN) model were made and presented. Best mix to create physical modeling of non-persistent rough joints was proposed. Using this mixture some blocks with non-persistent joints were created. The effect of non-persistent joint parameters on strength behavior of rock-like blocks were studied and the capability of the produced synthetic rock-liked material for the investigation of crack propagation under uniaxial loading condition was studied.

2. Materials and Methods

In this study, an appropriate artificial material is produced using plaster, cement, water and several additives. The most important characteristics of this material are: brittleness and relatively enough gelation time for providing non-persistent joints easily and relatively high strength in comparison to pure plaster. However, a combination of plaster and cement is normally used as a model material for simulating weak rocks. This mixture is applied due to its easily casting, flexibility, short setting time, low cost, and availability [20-21]. Furthermore, its higher unconfined compression strength in comparison with pure plaster and pure cement makes it a suitable material for modeling a jointed rock medium.

2.1. Cylindrical Specimen Preparation

A mixture of plaster and cement (type II), was utilized to prepare rock-like specimens. To do so at the first step, water content was determined to be 40 wt. % (wt. % means mass percentage). Therefore, 60 wt. % of mixture was made of solid (combination of plaster and cement). In the next step, the optimum value of P to achieve the highest UCS was investigated. Therefore, P was varied from 0 to 60 % of total mass and C from 60 to 0 %, simultaneously. Depending on mixture plan for each specimen 200 to 300 gr of plaster and cement were mixed thoroughly with 200 to 300 ml (40% by weight) of water to form a uniform paste. The specimen was prepared by pouring the mixture in the mold. The mold is an axially cracked cylinder with the internal diameter of 54 mm and height of 160 mm, fastened by clamps. Its base was adhered on a steel plate (Figure 1a). The mold was shaken by a vibrating table machine for approximately 2 minutes to achieve appropriate compaction and departure of air bubbles. The specimens were split by the length of 120±1 mm and kept in 25°c temperature for 1- 28 days, depending on the objective. (Figure 1b)

Figure 1. a) The molds for specimen preparation b) The prepared specimens.

2.1.1. Optimum Mix Plan

Since this material was to be used to investigate the effect of joint roughness on the mechanical response of specimens, it was required to possess a relatively high strength compared to pure plaster cylinders. The effect of plaster content on unconfined compression strength of prepared specimens at different ages is presented in Figure 2. Where P = 0 indicates that P = 0 wt % while at the same time C = 60 wt % and W = 40 wt % and P = 10 indicates that P = 10 wt %, C = 50 wt % and W = 40 wt % and so on. Samples with seven different plaster contents including 0, 10, 20, 30, 40, 50 and 60% were tested at different ages of 1, 3, 7, 14 and 28 days.

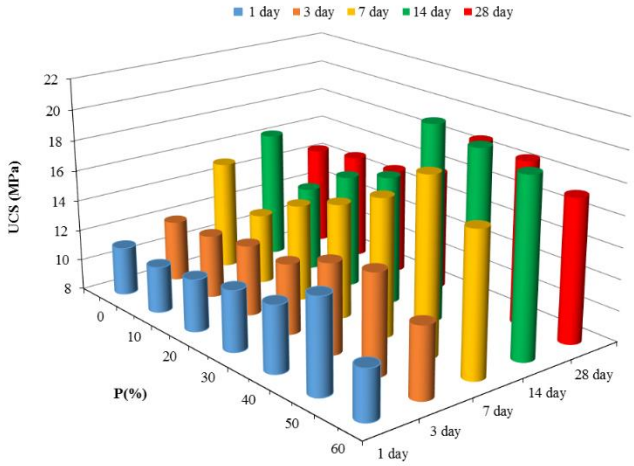

Figure 2. The effect of the P content on UCS of specimens with different ages.

The best mixture plan, as illustrated in Figure 2, is a combination of P = 40%, C = 20% and W = 40% which results in a UCS of 20.67 MPa. Therefore, in order to achieve the highest UCS, the P/C ratio of 2 is determined. Consequently, as presented in Figure 3, the effect of water content on UCS of specimens with P/C=2 was examined. Hence, three specimens with W= 35, 40 and 45% were investigated.

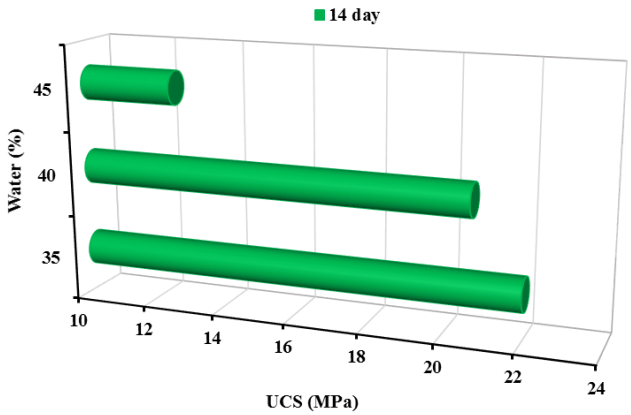

Figure 3. The effect of water content on UCS (A: 14 days).

At W > 40% the UCS is sharply reduced while for W < 35% the paste could not be made properly. One can arrive to the conclusion that W = 40% is the optimized value.

To investigate the effect of water temperature on UCS, some specimens were prepared with different water temperatures ranging from 10°C to 35°C (Figure 4). The results showed that at 20-25°C UCS does not vary and it fits well with normal lab temperature.

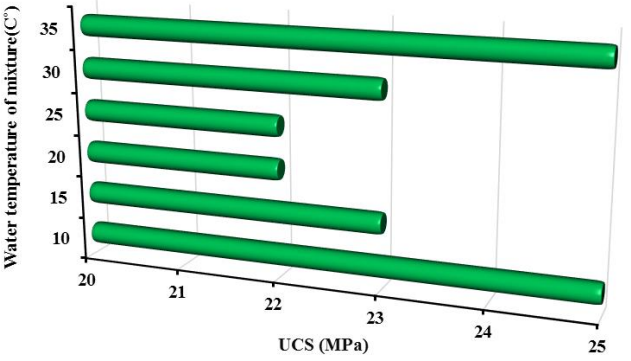

Figure 4. The effect of water temperature on UCS of cylindrical specimens (A: 14 days).

2.2. The Mix Plan for Blocky Specimens

The optimum mixture plan is used for blocky specimens (300 mm high, 300 mm wide, and 120 mm thick). Ten minutes of blending is required to make a uniform mixture. In the process of making blocky specimens, high amount of water content (i.e. W = 40%) and blending of the constituents for a long time bring about a reduction in UCS. The uniaxial strength of cylindrical specimens is 21 MPa, while UCS of blocky specimens with the same mixture is 6 MPa. Furthermore, the gelation time of this mortar (the interval between first and second setting times) is too short for making non-persistent joints. Therefore, some retardant and lubricant agents shall be used to prepare blocky specimens with relatively high UCS. At the first stage, the "Pardis Retarder" was examined for increasing the gelation time. The relationships between retardant and gelation time vs. UCS of cylindrical specimens are shown in Figure 5. As it can be seen, using 0.05% retardant (by weight of the total mixture) not only increased the gelation time of the mixture from 2 to 12 minutes but also increased the uniaxial compression strength of cylindrical specimens from 20.67 to 24 MPa.

For producing the blocky specimens, at least 10 minutes gelation time is needed; therefore according to Figure 5, 0.05wt% retardant with 12 minutes gelation time is chosen. On the other hand, lubricant can reduce the water content of the mixture, which in turn increases the solid content and fluidity. In this study, two commercial brands of lubricants (MGAR102 and MGAR106) were examined. In order to achieve maximum UCS, 3% lubricant by weight of plaster shall be used, as suggested by the lubricant producer. Therefore, three configurations of these lubricants were tested on blocky specimens and the results of which are presented in Table 1. As it can be seen, using 3% of the lubricant MGAR106 is suitable to increase the specimen strength. Using 3% lubricant, brought about a decrease in water content from 40 to 27.5%, an increase in plaster from 40 to 48.33% and an increase in the cement content from 20 to 24.17%.

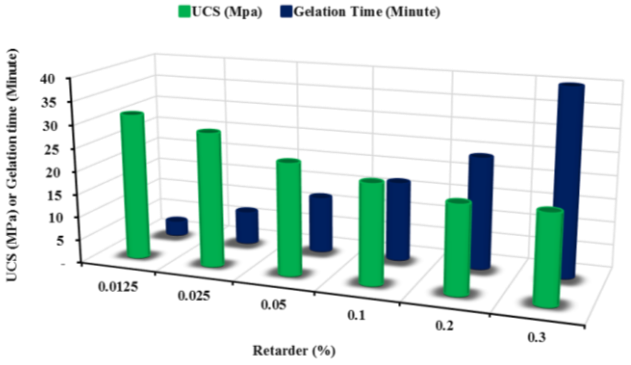

Figure 5. The effect of retardant on gelation time and UCS of cylindrical specimens (A: 14 days).

Table 1. The effect of two different lubricants on the uniaxial compression strength of blocky specimens (A: 14 days).

Parameter	Test set 1	Test set 2	Test set 3
Lubricant MGAR106 (%)	3	1.5	0
Lubricant MGAR103 (%)	0	1.5	3
UCS (MPa)	22.97	20.17	18.11

The best configuration is using 3 wt% MGAR106 lubricant, which results in the UCS of 23.06 MPa. By using the lubricant MGR106, the blending time for preparation of the mixture and water content were reduced from 10 minutes and 40% to 4 minutes and 27.5% respectively. Finally, it should be mentioned that the combination of retardant and MGAR106 factor extends the gelation time of mortar from 12 minutes in cylindrical specimens and to 14 minutes in blocky specimens. This is very helpful and necessary to create non-persistent mated joints. On the contrary, without these two additives the gelation time of mortar decreases to less than 2 minutes which renders the creation of non-persistent mated joints impossible.

2.3. Mechanical Properties of Intact Specimens

In order to determine the mechanical properties of artificial material, laboratory tests such as UCS, triaxial and Brazilian tests were conducted on cylindrical and blocky specimens. A summary of mechanical properties of specimens is listed in Table 2.

Table 2. Mechanical properties of rock-like specimens.

Parameter	Cylindrical specimen	Blocky specimen
σ_c (MPa)	23.70	22.97
E (GPa)	10.53	3.78
σ_t (MPa)	3.43	-
Poisson's ratio	0.17	-
Cohesion (MPa)	10.99	-
Internal friction angle (degree)	23.95	-

It should be noted that the word brittleness is not a property but a behavior and there is not any agreement between researchers on which number a specimen can be called brittle or ductile [22]. Therefore, rather than using a number as brittleness index, the dropping behavior of the UCS after peak load was what this research was looking for and this specimen seemed to meet this behavior. The dropping behavior of the UCS after the peak load in stress-strain curves of cylindrical and blocky specimens are illustrated at Figure 6. This figure indicated the prepared specimen was brittle enough to be used for modeling of

cracking behavior.

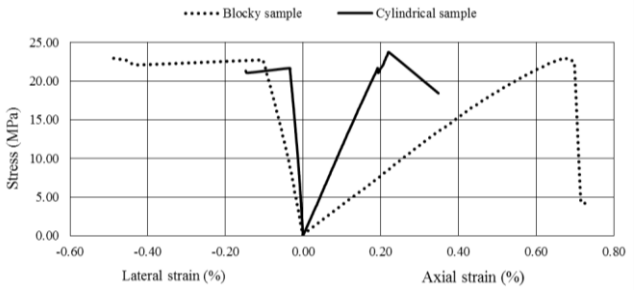

Figure 6 Stress-strain curves for cylindrical and blocky specimens.

2.4. Jointed Specimen Preparation

2.4.1. JRC Sheets

The joints were created using 3D JRC sheets with dimensions of 150 × 100× 1 mm as presented in Figure 7. 3D JRC sheets were prepared using digitizing the standard JRC profiles proposed by Barton. The sheets are designed according to the digitized profiles utilizing SolidWorks software and created using a 3D printer. The mechanical properties of JRC sheets are presented in Table 3.

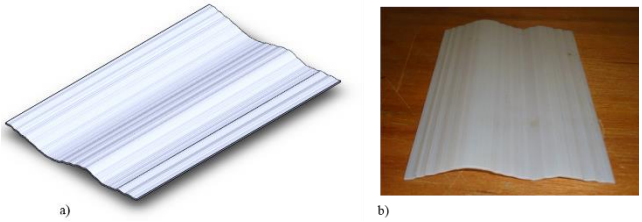

Figure 7. 3D JRC sheet of Barton (JRC, 14-16), a) designed by SolidWorks b) prepared by 3D printer.

Table 3. Mechanical properties of JRC sheets (All units in MPa).

Material	σ_{ci}	E_i	Tensile strength	Flexural strength	Flexural modulus
Vero-Gray	85.5	3000	60	95	3000

2.4.2. The Cast for Preparing Non-Persistent Jointed Specimens

Some identical specimens were made by designing the cast in such a way to have high flexibility for a wide range of non-persistent joint parameters (Figure 8). The cast has three parts as follows: 1) frame: consisting of a box and upper platform; 2) T-shaped segment: which is held by upper platform and is connected to the L-shaped segment, and finally 3) a pair of the L-shaped parts on which JRC sheets are assembled. The components of cast were as follows:

1. The main box: the bottom of the main box and the walls were made of steel and Plexiglas, respectively. They were connected by bolts at the bottom of the box. The dimensions of the box are 300 × 300 × 120 (in millimeters).
2. Bolt rail: on each wall, a profile has been mounted on which the head of a bolt can easily move. These profiles act as a rail for the bolt. A ruler has also been installed on these profiles to control the joint inclination (θ) utilizing the x-y coordinate system.
3. The upper platform: assembled on the box using two rods.
4. Protractor: installed on the upper platform to control the bridge angle (γ).
5. T-shaped segment: there is a hole on the upper platform in which the T segment can be easily rotated in order to measure the rotation along the protractor through a mounted pointer. On the lower part of the T segment as well, there is a sliding rail on which the head of the L segment can easily move, and a ruler which helps in controlling the length of the bridge.
6. The head of the L segment: this part can easily slide on the sliding rail of T segment and it can be fixed using two bolts installed in the upper and lower parts. The head and the other part of the L segment can easily rotate around the lower bolt.
7. The L segment: it is placed on a sliding rail-like profile and has a notch in its lower part. This segment can easily move in *x* and *y* directions using a bolt located on the abovementioned rail.
8. The notch: JRC sheet is easily seated in the second notch (number 8 in Figure 8). There is a set of jaws that hold the JRC sheet On top of this notch. Two sets of bolts on the top can fix these jaws.
9. The JRC sheets: these sheets can be held by the lower part of L segment.

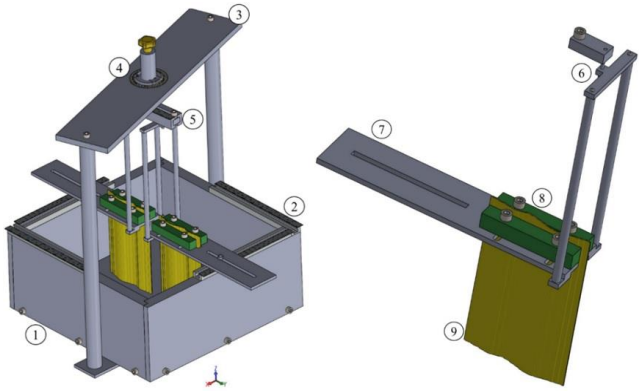

Figure 8. Schematic view of designed cast for pre-creation of non-persistent jointed specimens.

2.5. Preparation of Non-Persistent Jointed Specimens

After complete adjustment of cast regulation and joint pattern (at the bottom of the cast), and correctly setting of the upper and lower parts of JRC sheets, the cast would be ready for pouring the mortar (Figure 9a). The mortar was gently poured in the cast after it was carefully mixed. Keeping JRC sheets unmoved is very crucial. In this regard, two actions has to be done simultaneously: 1) the mortar should be poured very slowly and gently from the corners of the cast; 2) a normal load on the JRC sheets must be applied, until the cast is completely full. The mortar was thoroughly mixed for 12 minutes and while it started hardening the sheets were removed simultaneously. The critical part of this process was the removal time of JRC sheets. Too early removing of the sheets results in gluing the joint surfaces to each other and inheriting high cohesion. On the other hand, if the removal time of the sheets exceed 14 minutes, the sheets will stick into the specimen and could not be removed. This could resulted in the loss of a specimen. Figure 9b presents non-persistent joint with JRC 0-2.

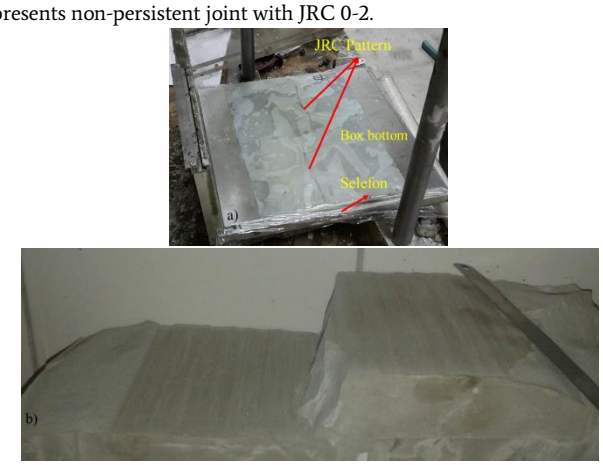

Figure 9. Non-persistent jointed specimen: a) Pattern of joints at the bottom of the cast; b) Step non-persistent jointed specimen (JRC, 0-2).

In the following section, attempts have been done to formulate the UCS of cylindrical specimens in the terms of P and A using MNR modeling.

3. Multivariate Non-Linear Regression Analysis

MNR is an extension of the regression analysis that includes additional independent variables in the predictive equation. Nonlinear regression is appropriate when the relationship between the dependent and independent variables is not intrinsically linear. This method is employed to establish an empirical formula in order to predict the dependent variables based on the known independent variables [23]. Here, a relationship between unconfined compressive strength (output) and the other relevant parameters (inputs), that is, P and A has been discussed based on the multivariate non-linear regression. To generate multivariate relation on the basis of same database as considered for training the ANN model, the statistical software package SPSS21 was used. The analysis of variance (ANOVA) technique was applied to the results of the non-linear regression and its statistical parameters were attained as presented in Table 4.

Table 4. Analysis of variance.

	Model	Sum of squares	Degree of freedom	Mean square	R squared*
UCS	Regression	7925.178	3	2641.726	0.716
	Residual	74.803	32	2.338	
	Uncorrected Total	7999.980	35		
	Corrected Total	262.971	34		

* R squared = 1 - (Residual Sum of Squares) / (Corrected Sum of Squares)

The non-linear multiple regression (MNR) equation for UCS values found is as follows:

$$UCS = 1.752 Ln\, A + 10.031 e^{0.005P} \quad (1)$$

The regression analysis was done to formulate the UCS of rock-like material in terms of P and A. Since R2 of the suggested formula is not very good, the neural network analysis was done to predict UCS of cylindrical specimens in terms of P and A.

4. Artificial Neural Networks

Artificial neural networks are a form of artificial intelligence which is based on biological structure found in human brains. In the cases that the relations between inputs and outputs are unknown, ANN can be used to learn and compute the relations between them. In engineering problems, ANNs can be used to affirm and purify design solutions [24]. An ANN is a computing system consisting of highly interconnected set of simple information processing elements called neurons or perceptrons. The arrangement of these neurons determines the ANN architecture. A particular network is defined using three fundamental components: transfer function, network architecture, and learning law. One has to define these constituents depending on the problem to be solved [25, 26]. One of the most commonly implemented ANNs is Bayesian Regularization of Neural Networks (BRANN) technique.

4.1. Bayesian Regularization of Neural Networks

Bayesian regularized artificial neural networks (BRANNs) is one of the most commonly implemented ANNs. BRANNs are kind of back propagation learning approaches that are more powerful than conventional back-propagation networks and can omit at least decrease the necessity for lengthy cross-validation step. The back propagation ANN is a very popular method in the field of ANN that depends on supervised learning, typically via the use of a gradient descent method to reduce a chosen error function. General architecture of feed forward neural network are input, hidden and output layers. The connection between neurons in each layer is called a link (Figure 11). The measurement of the connection between two nodes is provided by these links that contain a weighted value. [27,28]. These weights are changed by the supervised learning method in order to decrease the arbitrary error function –usually mean square error- to enhance the network for use on unknown specimens. Overfitting and overtraining is a major issue in this technique, and each of them results in a fitting of the noise and a loss of generalization of the network. Bayesian regularization is a mathematical technique that was proposed in order to reduce the overfitting problem by converting nonlinear systems into 'well-posed' problems [29, 30]. Generally speaking the objective of training step is to minimize sum square error of the model output and target value. An additional term is added by BRANN to this equation:

$$F = \beta E_D + \alpha E_w \quad (2)$$

Where, F is the target function, ED is the sum of squared errors, Ew is the sum of square of the network weights, and a and b are target function parameters [30]. In BRANN the weights are considered random variables and thus their density function is written according the Baye's rules [31]:

$$P(w \mid D, \alpha, B, M) = \frac{P(w \mid D, \beta, M) P(w \mid \alpha, M)}{P(D \mid \alpha, \beta, M)} \quad (3)$$

Where, w is the vector of network weights, D represents the data vector, and M is the neural network model being used. Forsee and Hagan assumed that the noise in the data was Gaussian, and with this assumption they were able to determine the probability density function for the weights [31]. The optimization of the regularization parameters a and b demands for solving the Hessian matrix of F(w) at the minimum point wMP. They proposed a Gauss–Newton approximation to the Hessian matrix which is possible if the Levenburg–Marquardt training algorithm is used to locate the minimum [31]. This technique reduces the potential for arriving at local minimum, thus increasing the generalizability of the network. The novelty of this technique is the probabilistic nature of the network weights in relation to the given data set and model framework. As a neural network grows in size through additional hidden layer neurons, the potential for overfitting increases dramatically and the need for a validation set to determine a stopping point is crucial. In Bayesian regularized networks, overly complex models are penalized as unnecessary linkage weights are effectively driven to zero. The network will calculate and train on the nontrivial weights, which are also known as the effective number of parameters and which will converge to a constant value as the network grows [29]. The inherent noise and volatility of physical modeling data introduces a high probability of overfitting and overtraining for general back propagation networks. These more parsimonious networks reduce the chance of overfitting while eliminating the need for a validation step, thus increasing the available data for training.

4.2. Data Collection and Preparation

Data collection is one of the most important steps in ANN modeling. Here, 35 specimens were made with different ratios of plaster and cement. The specimens with different ages were tested. The data collection was made using physical testing. In these experiments, the independent variables namely P/C ratio and the age of specimens were introduced based on P (plaster content percentage) and the day of testing after specimen preparation. In addition the dependent variable were defined to be uniaxial compression strength of specimens (UCS). The list of the data collected is presented in Table 5.

4.3. Determination of Optimum Network

The optimum architecture of BRANN model can be determined by testing different types of networks based on trial and error. Therefore, root mean square error (RMSE) is evaluated for all models, and accordingly, the model with minimum RMSE was chosen as the optimum model. The optimum number of neurons in hidden layers was also obtained by trial and error based on the minimum RMSE. The network performance for different numbers of neurons in hidden layers is depicted in Figure 10. As it is illustrated in the figure, to determine the optimum number of hidden neuron, nine networks with different number of neurons in hidden layers were examined. The optimum neurons can be located in one or two hidden layers that their arrangements must be determined. According to Figure 10, a network with 8 neurons in hidden layers had the best performance in comparison with the others.

Table 5. The list of the collected data.

No.	Specimen age (in ay)	P (%)	UCS (MPa)
1	1	0	11.13
2	1	10	11.00
3	1	20	11.40
4	1	30	11.95
5	1	40	12.30
6	1	50	14.08
7	1	60	11.22
8	3	0	11.95
9	3	10	12.10
10	3	20	12.58
11	3	30	12.58
12	3	40	13.83
13	3	50	14.46
14	3	60	12.58
15	7	0	15.09
16	7	10	12.58
17	7	20	14.29
18	7	30	15.43
19	7	40	16.91
20	7	50	19.35
21	7	60	17.21
22	14	0	16.29
23	14	10	13.52
24	14	20	15.34
25	14	30	16.32
26	14	40	20.67
27	14	50	20.12
28	14	60	19.49
29	24	0	14.46
30	24	10	14.90
31	24	20	14.95
32	24	30	15.72
33	24	40	18.79
34	24	50	18.52
35	24	60	17.27

In the next step, according to the optimum number of neurons in hidden layers, RMSE was calculated for different types of the models including one and two hidden layers with different number of neurons and transfer functions (Table 6). RMSE is calculated by equation (3) [32]:

$$RMSE = \sqrt{\frac{1}{N}\sum_{i=1}^{n}(u_k - u_k)^2} \quad (3)$$

Which, u_k and u_k are the k_{th} predicted and observed values of target, respectively.

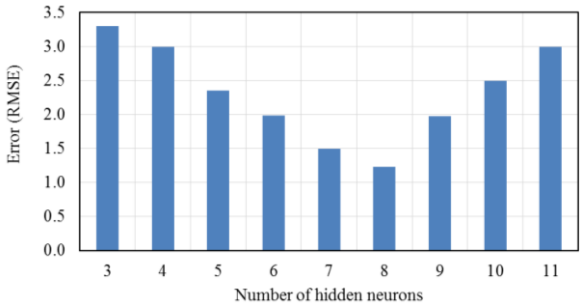

Figure 10. Network performances for different numbers of neuron in hidden layers.

As it can be seen from Figure 10 and Table 6, the network with architecture 2-6-2-1 and TANSIG transfer function had the minimum RMSE, hence it was considered as the optimum model.

Table 6. Results of some models with different architecture and transfer functions.

No.	Network architecture	RMSE (Transfer function, TANSIG)	RMSE (Transfer function, LOGSIG)
1	2-8-1	1.58	1.74
2	2-7-1-1	1.37	1.98
3	2-6-2-1	1.11	1.15
4	2-5-3-1	1.23	1.35
5	2-4-4-1	1.53	2.35

Figure 11. shows a graphical presentation of this network. Also, the whole information of optimum network architecture is given in Table 7.

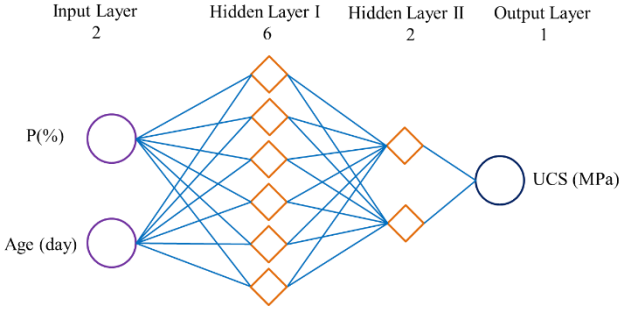

Figure 11. Suggested BRANN architecture for the UCS prediction.

Table 7. Full information of the optimum network architecture.

Number of input neurons	2
Number of hidden layers	2
Number of hidden neurons	8
Number of output neurons	1
Number of training epochs	300
Number of training datasets	25
Number of testing datasets	10
Training function	Bayesian Regularization
Transfer function	TANSIG
Learning rate	0.1
Error goal	0

Approximately 30 % of the dataset was randomly chosen to test the optimum ANN model. These data were not used in the training of the network. This leads to test the ANN application in a more versatile manner. The results of the network are presented in this section to demonstrate its performance. Correlation coefficient between the predicted and measured values of UCS is taken as the network

performance. The prediction was based on the input datasets that were discussed in the previous section. Figure 12 shows the results for optimum network in terms of correlation coefficient for training and testing processes.

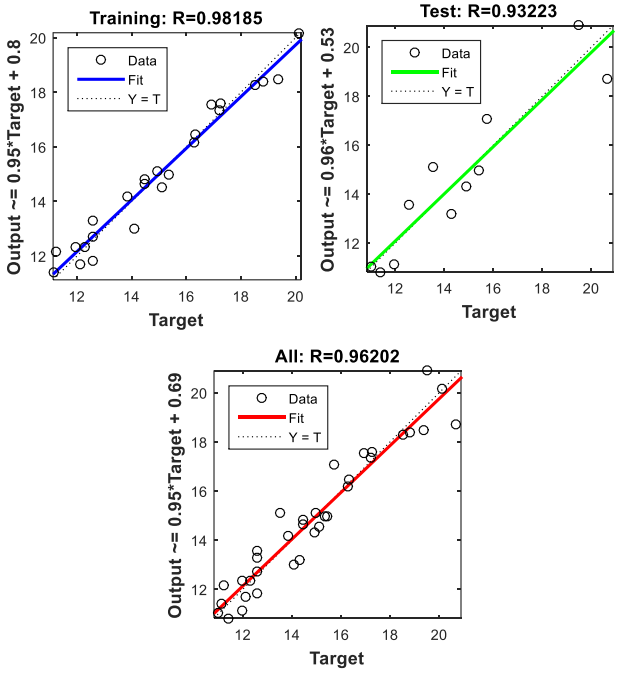

Figure 12. Results of the optimum neural network model.

5. Comparison of Models Performance

The performance of MNR and BRANN models were evaluated using variance accounted for (VAF), root mean square error (or RMSE as described in Equation 3), mean absolute error (MAE) and the coefficient of efficiency (CE), defined as follows:

$$VAF = 100\,(1-\frac{var(u_k - u_k)}{var(u_k)}) \quad (5)$$

$$MAE = \frac{1}{N}\sum_{k=1}^{N}\left|u_k - u_k\right| \quad (6)$$

$$CE = 1-\frac{\sum_{k=1}^{N}(u_k - u_k)^2}{\sum_{k=1}^{N}(u_k - \bar{u})^2} \quad (7)$$

Where, var denotes variance; u_k and u_k are already introduced in this research; $\bar{u}$ is the mean of predicted target values; and N is the number of observations for which the error has been computed. VAF index displays the degree of difference between the variances of measured and predicted datasets. VAF values closer to 100% indicate low variability and consequently better prediction capabilities. RMSE index is the measure of bias between measured and predicted data. The lower the RMSE, the better the model performs [18,25,26]. Ideally, the value of RMSE and MAE should be zero and that of CE should be one. The relevant outputs were controlled with performance indices. A comparison between models performances indexes is presented in Table 8.

For testing the models, 10 datasets that were not incorporated into the development of the models were used. Based on the testing data, the models performance indices were calculated and summarized in Table 8. Also, comparison between predicted and measured UCS for BRANN and MNR models are shown in the Figures 13 and 14, respectively. It can be seen from the comparisons that the performance of BRANN model in terms of those indices is much better than MNR model and its results are closer to the real-world data.

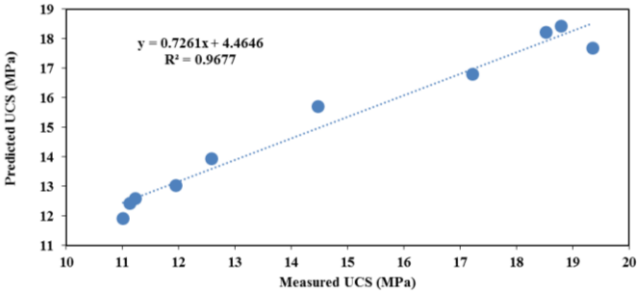

Figure 13. Comparison between the measured and predicted UCS for the ANN model.

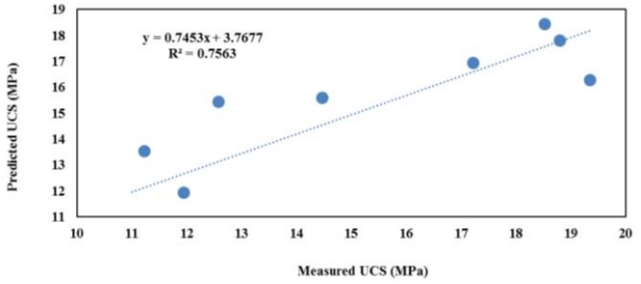

Figure 14. Comparison between measured and predicted UCS for the MNR model.

Table 8. A comparison between average performance indices of MNR and BRANN models.

Index	MNR model	BRANN model
R^2	75.63	96.77%
VAF (%)	75.62	90.74
RMSE	1.64	1.11
MAE	1.23	1.01
CE	0.67	0.79

6. Sensitivity Analysis

Sensitivity analysis was performed on the output of the models in order to recognize the input parameters with the most significant impact on the average output parameter. Cosine amplitude method was used to investigate similarity relations between the interconnected parameters (CAM) [18, 33, and 34]. In this method, the data pairs are expressed in a common X-space and used to construct a data array X which is defined as:

$$X = \{X_1, X_2, X_3, \ldots X_m\} \quad (8)$$

Each elements (X_i) in the data array X is a vector of lengths and expressed as follows:

$$X_i = \{x_{i1}, x_{i2}, x_{i3}, \ldots, x_{im}\}_1 \quad (9)$$

Therefore, in this method each data pairs is considered as a point in m-dimensional space, where each point requires m-coordinates for a full description. Each element of the (r_{ij}) relation results a pairwise comparison of two data pairs. The strengths of relations (r_{ij}) between output and input parameters can be calculated as follows:

$$r_{ij} = \sum_{k=1}^{m} x_{ik}x_{jk} \Big/ \sqrt{\sum_{k=1}^{m} x_{ik}^2 \sum_{k=1}^{m} x_{jk}^2} \quad (10)$$

Figure 15 shows the strength values of relations (rij) between input parameters and UCS for BRANN and MNR models. As it is depicted in Figure 15, according to the results of both models, plaster content had a more pronounced influence on UCS than specimen age had.

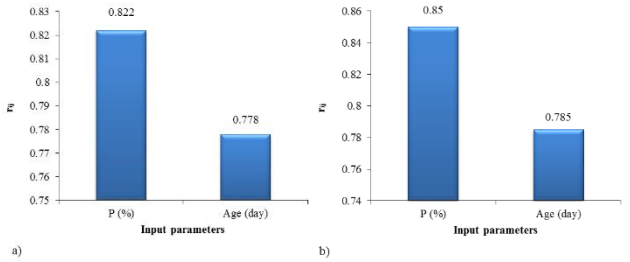

Figure 15. Strength of relationship (rij) between UCS and input parameters a) BRANN model b) MNR model.

7. UCS Tests on Blocky Specimens

7.1. Setup and Testing Procedure

The tests were carried out using a Material Testing Machine (MTS) under displacement controlled condition. For the UCS tests, the normal and constant velocity of 0.005 mm/s was controlled by the MTS machine. The load was applied to the specimen using two steel plates. In order to neutralize the effect of friction between these steel plates against the specimen, Teflon sheets of 2 mm thickness were used. A view of non-persistent joint parameters and loading condition is illustrated in Figure 16.

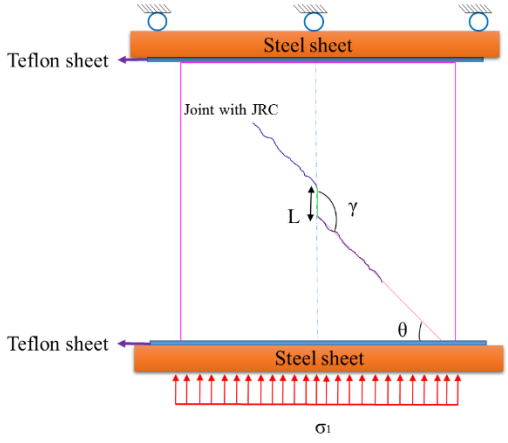

Figure 16. Joint configuration and boundary condition in uniaxial compressive loading.

7.2. Physical Experiments Setup

The physical tests were designed using Response Surface Methodology (RSM) which is some sort of experiment design method. A total Central Composite Design (CCD) experiment contained 30 points in which 24 points were factorial points and the remaining 6 points were zero points used to estimate the experimental error. The results of this method have been presented elsewhere. Some specimens of the CCD experiment used in this research are presented in Table 9.

7.3. Effect of Non-Persistent Joint Parameters on the Strength Behavior of the Blocks

The effect of joint inclination (θ), Joint Roughness Coefficient (JRC), bridge angle (γ) and bridge length (L) on the strength behavior of jointed blocks was investigated using physical modeling. While studying the effect of one parameter, the other parameters were kept constant at their average value.

7.3.1. Joint Inclination (θ)

The effect of θ on the σ_c was investigated by varying this parameter from 0° to 90°. The physical models were tested with θ of 0°, 45° and 90°. The results showed that as joint inclination increases from 0° to 60°, σ_c decreases; and but when θ increases from 60° to 90°, uniaxial compression strength increases (Figure 17). Indeed, UCS takes its minimum at joint inclination of 60º. It should be noted that, as θ takes values less than 30°, the stress concentration at joint tips decreases and stress distributes more uniformly over the rock bridges. This leads to an increase in σ_c.

Table 9. CCD experimental results of the specimens used in this investigation.

Specimen code	JRC	L (mm)	γ (degree)	θ (degree)	σ_{cj} (MPa)
U1	10	25.0	135.0	0.0	21.66
U2	0	25.0	135.0	45.0	15.00
U5	20	25.0	135.0	45.0	19.03
U11	10	25.0	135.0	45.0	17.01
U12	10	25.0	135.0	45.0	16.21
U14	10	25.0	180.0	45.0	18.88
U15	10	25.0	135.0	45.0	16.44
U18	10	25.0	135.0	45.0	16.04
U19	10	25.0	135.0	90.0	17.60
U20	10	25.0	90.0	45.0	13.90
U21	10	10.0	135.0	45.0	15.50
U27	10	25.0	135.0	45.0	16.55
U29	10	40.0	135.0	45.0	18.52
U30	10	25.0	135.0	45.0	16.78

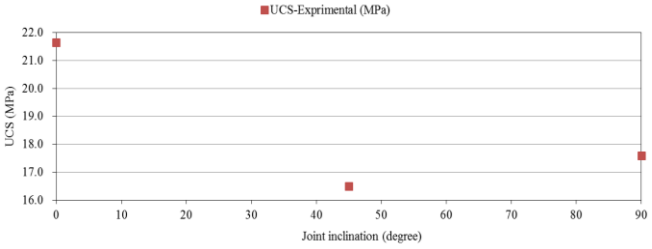

Figure 17. Effect of joint inclination on σ_c.

7.3.2. JRC

The effect of JRC was investigated by varying this parameter from 0-2 to 18-20. JRC was taken to be 0-2, 10-12 and 18-20 in physical models. The effect of JRC on σ_c is shown in Figure 18. The results indicate that as the JRC increases, σ_c increases as well.

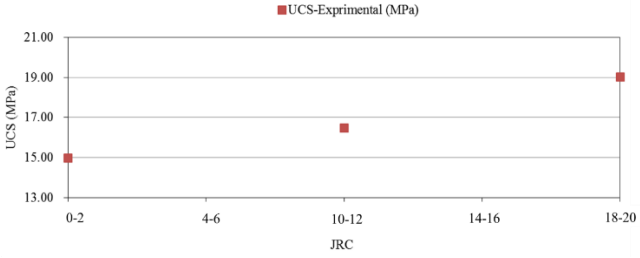

Figure 18. Effect of JRC on σ_c.

7.3.3. Bridge Angle (γ)

The effect of bridge angle (γ) on σ_c was studied by altering the value of this parameter from 90° to 180°. The physical model was tested with γ of 90°, 135° and 180°. The results indicate that as γ increases σ_c increases as well (Figure 19).

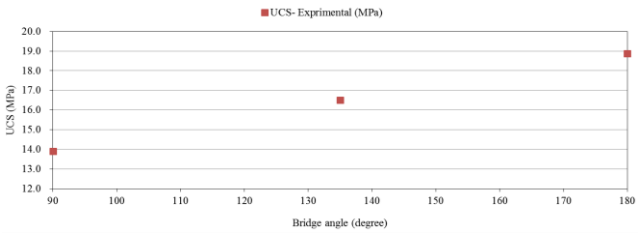

Figure 19. Effect of bridge angle on σ_c.

7.3.4. Bridge Length (L)

To consider the effect of bridge length on σ_c, bridge length was varied from 10 mm to 50 mm. Bridge length was taken 10 mm, 25 mm and 40 mm in physical models. The effect of bridge length on uniaxial compressive strength is shown in Figure 20. The results indicate that as the length increases σ_c increases as well.

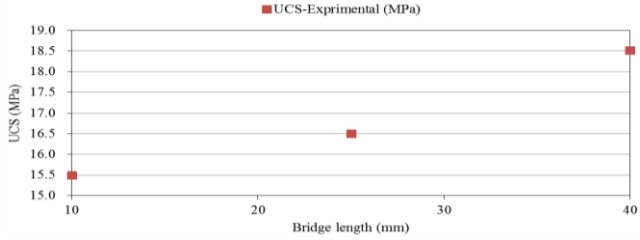

Figure 20. Effect of bridge length on σ_c.

Although the investigation of crack initiation, propagation and coalescence of non-persistent joints is out of the scope of this paper and the discussion of this issue is presented elsewhere, but in this section just as an example, the crack initiation, propagation and coalescence of specimen U30 which is a central point in the CCD experiment design is presented in Figure 21. This example indicates that the produced synthetic rock-like material is good enough to model crack development under uniaxial compressive loading.

Figure 21. Specimen U30 (θ=45°) a) before test and initiation of outer crack tips b) crack coalescence in the bridge area c) after test d) schematic view of the propagated cracks.

8. Conclusions

In this paper, a synthetic rock-like material was produced to physically model weak rocks. This material is appropriate to investigate the effect of non-persistent joint parameters on mechanical behavior of blocky specimens. The effect of parameters such as plaster content, cement content, specimen age, retardant and lubricant on the UCS of small specimens were investigated. An MNR and a BRANN model were developed to predict UCS of cylindrical specimens based on plaster content and specimen age. Finally, the effect of joint inclination (θ), Joint Roughness Coefficient (JRC), bridge angle (γ) and bridge length (L) on the strength behavior of jointed blocks was investigated using physical models. The following key conclusions can be drawn.

1. In cylindrical specimens, the highest UCS=20.67 MPa was obtained by combination of W=40%, P=40% and C=20%. The UCS of blocky specimens with this mixture plan measured at 6 MPa. This reduction happened mainly due to long mixing time and high amount of paste water content. In addition, the gelation time of this mixture plan was so short (about 1 to 2 minutes) and this time is not enough to produce non-persistent jointed specimens.
2. The water temperature in mixture affects the UCS of specimens. In order to remove the impact of temperature variation of paste water on UCS, the water temperature was kept constant in the range of 20C° to 25C°, which is equivalent to the normal room temperature. In this temperature interval, UCS had minimum variation.
3. Using retardant increased the gelation time of the mixture and decreased the unconfined compression strength of the specimen simultaneously. Therefore, using 0.05 % retardant (by the weight of the mixture) increased the gelation time of the mixture from 2 to 12 minutes. Furthermore, using retardant and lubricant in blocky samples increased gelation time up to 14 minutes.
4. By reducing the water content and increasing solid content and fluidity of the mixture, lubricant resulted in an increase in the UCS of blocky specimens. Using 3% lubricant MGAR106 (by the weight of plaster) resulted in an increase of 8.33 % plaster, 4.17% cement content and a decrease of water content of 12.5%. These all in turn yielded an increase of 284.3% in block strength.
5. The effect of P and specimen age on UCS of cylindrical specimens was examined. Based on these two parameters, a Bayesian regularization neural network model and a multivariate non-linear regression model were developed to predict UCS of cylindrical specimens. The average performance of proposed models was evaluated by the following indices: variance account for (VAF), root mean square error (RMSE), mean absolute error (MAE), coefficient of efficiency (CE), and coefficient of correlation (R2). The optimum average performance of the BRANN and MNR models was verified by the calculated values of VAF, RMSE, MAE, CE , R2 as 90.74%, 1.11, 1.01, 0.79, 96.77 % and 75.62%, 1.64, 1.23, 0.67, 75.63% respectively for both models. The results obtained from this study indicate that the developed BRANN model can generalize complex nonlinear relationships between UCS and P content and specimen age. This showed that BRANN model can provide a more accurate prediction for UCS values than MNR model does.
6. Sensitivity analysis was conducted on the inputs of both models. The results of the cosine amplitude method (CAM) showed that P had the most noticeable impact on UCS of cylindrical specimens.
7. The results of this research showed that the produced rock-like material with properties of P/C=2, W=27. 5% of the weight of the mixture, 3% MGAR106 factor by the weight of plaster and 0.05% of the weight of the solid is suitable to physically model mechanical and cracking behavior of non-persistent jointed specimens subjected to uniaxial compressive load.
8. Uniaxial strength takes its minimum at θ=60º when joint angle is varied. The maximum UCS is provided when θ = 0º.
9. Increasing each of JRC, bridge length and bridge angle parameters of a non-persistent joint while other properties unchanged, increases the compressive strength of blocky specimens.

REFERENCES

[1] Bobet, A., & Einstein, H. H. (1998). Fracture coalescence in rock-type materials under uniaxial and biaxial compression. International Journal of Rock Mechanics and Mining Sciences, 35(7), 863-888.

[2] Bobet, A. (2000). The initiation of secondary cracks in compression. Engineering Fracture Mechanics, 66(2), 187-219.

[3] Wong, R. H. C., & Chau, K. T. (1997). The coalescence of frictional cracks and the the shear zone formation in brittle solids under compressive stresses. International Journal of Rock Mechanics and Mining Sciences,34(3), 335-e1.

[4] Wong, R. H. C., Chau, K. T., Tang, C. A., & Lin, P. (2001). Analysis of crack coalescence in rock-like materials containing three flaws—part I: experimental approach. International Journal of Rock Mechanics and Mining Sciences, 38(7), 909-924.

[5] Park, N. S. (2001). Crack propagation and coalescence in rock under uniaxial compression. Seoul: Seoul National University.

[6] Sagong, M., & Bobet, A. (2002). Coalescence of multiple flaws in a rock-model material in uniaxial compression. International Journal of Rock Mechanics and Mining Sciences, 39(2), 229-241.

[7] Gehle, C., & Kutter, H. K. (2003). Breakage and shear behaviour of intermittent rock joints. International Journal of Rock Mechanics and Mining Sciences, 40(5), 687-700.

[8] Li, Y. P., Chen, L. Z., & Wang, Y. H. (2005). Experimental research on pre-cracked marble under compression. International Journal of Solids and Structures, 42(9), 2505-2516.

[9] Prudencio, M., & Jan, M. V. S. (2007). Strength and failure modes of rock mass models with non-persistent joints. International Journal of Rock Mechanics and Mining Sciences, 44(6), 890-902.

[10] Ghazvinian, A., Nikudel, M. R., & Sarfarazi, V. (2007, August). Effect of rock bridge continuity and area on shear behavior of joints. In The Second Half Century of Rock Mechanics, Three Volume Set: 11th Congress of the International Society for Rock Mechanics, 3 VOLUMES+ CD-ROM (Vol. 1, p. 247). CRC Press.

[11] Wong, L. N. Y., & Einstein, H. H. (2009). Crack coalescence in molded gypsum and Carrara marble: part 1. Macroscopic observations and interpretation. Rock Mechanics and Rock Engineering, 42(3), 475-511.

[12] Wong, L. N. Y., & Einstein, H. H. (2009). Crack coalescence in molded gypsum and Carrara marble: part 2—microscopic observations and interpretation. Rock Mechanics and Rock Engineering, 42(3), 513-545.

[13] Park, C. H., & Bobet, A. (2009). Crack coalescence in specimens with open and closed flaws: a comparison. International Journal of Rock Mechanics and Mining Sciences, 46(5), 819-829.

[14] Huang, Y. H., Yang, S. Q., Tian, W. L., Zeng, W., & Yu, L. Y. (2015). An experimental study on fracture mechanical behavior of rock-like materials containing two unparallel fissures under uniaxial compression. Acta Mechanica Sinica, 1-14.

[15] Kumar BR, Vardhan H, Govindaraj M, Vijay GS. (2013). Regression analysis and ANN models to predict rock properties from sound levels produced during drilling. International Journal of Rock Mechanics and Mining Sciences. 58,61-72.

[16] Ali E, Guang W, Ibrahim A. (2014) Empirical relations between compressive strength and microfabric properties of amphibolites using multivariate regression, fuzzy inference and neural networks: A comparative study. Engineering Geology. 183,230-40.

[17] Majdi A, Rezaei M.(2013). Prediction of unconfined compressive strength of rock surrounding a roadway using artificial neural network. Neural Computing and Applications. 23(2),381-9.

[18] Asadizadeh M, Hossaini MF. (2016). Predicting rock mass deformation modulus by artificial intelligence approach based on dilatometer tests. Arabian Journal of Geosciences. 9(2),1-5.

[19] Mohammad R, Mostafa A, Abbas M, Farouq HM. (2015). Prediction of representative deformation modulus of longwall panel roof rock strata using Mamdani fuzzy system. International Journal of Mining Science and Technology. 25(1), 23-30.

[20] Ghazvinian, A., Sarfarazi, V., Schubert, W., & Blumel, M. (2012). A study of the failure mechanism of planar non-persistent open joints using PFC2D.Rock mechanics and rock engineering, 45(5), 677-693.

[21] Ghazvinian, A., Nejati, H. R., Sarfarazi, V., & Hadei, M. R. (2013). Mixed mode crack propagation in low brittle rock-like materials. Arabian Journal of Geosciences, 6(11), 4435-4444.

[22] Hucka, V., & Das, B. (1974, October). Brittleness determination of rocks by different methods. In International Journal of Rock Mechanics and Mining Sciences & Geomechanics Abstracts (Vol. 11, No. 10, pp. 389-392). Pergamon.

[23] Jennrich, R. I. (1995). An Introduction to computational statistics regression analysis. Prentice Hall, Englewood Cliffs, NJ.

[24] Mert, E., Yilmaz, S., & İnal, M. (2011). An assessment of total RMR classification system using unified simulation model based on artificial neural networks. Neural Computing and Applications, 20(4), 603-610.

[25] Simpson, P. K. (1990). Artificial neural system—foundation, paradigm, application and implementations. New York, Pergamon.

[26] Kosko, B. (1992). Neural networks and fuzzy systems: a dynamical systems approach to machine intelligence/book and disk. Vol. 1Prentice hall.

[27] Garson, D. G. (1991). Interpreting neural network connection weights.

[28] Goh, A. T. C. (1995). Back-propagation neural networks for modeling complex systems. Artificial Intelligence in Engineering, 9(3), 143-151.

[29] Ticknor, J. L. (2013). A Bayesian regularized artificial neural network for stock market forecasting. Expert Systems with Applications, 40(14), 5501-5506.

[30] MacKay, D. J. (1992). A practical Bayesian framework for backpropagation networks. Neural computation, 4(3), 448-472.

[31] Foresee, F. D., & Hagan, M. T. (1997, June). Gauss-Newton approximation to Bayesian learning. In Neural Networks, 1997., International Conference on(Vol. 3, pp. 1930-1935). IEEE.

[32] Tzamos, S., & Sofianos, A. I. (2006). Extending the Q system's prediction of support in tunnels employing fuzzy logic and extra parameters. International Journal of Rock Mechanics and Mining Sciences, 43(6), 938-949.

[33] Grima, M. A. (2000). Neuro-fuzzy modeling in engineering geology. AA Balkema, Rotterdam, 244.

[34] Ross, T., (1995). Fuzzy logic with engineering applications. New York: McGraw-Hill Inc.